

# The Production of H I in Photodissociation Regions and A Comparison with CO(1–0) Emission

Ronald J. Allen

*Space Telescope Science Institute  
3700 San Martin Drive, Baltimore, MD 21218;  
rjallen@stsci.edu*

Harold I. Heaton

*Johns Hopkins University, Applied Physics Laboratory  
11,100 Johns Hopkins Road, Laurel, MD 20723;  
Hal.Heaton@jhuapl.edu  
and*

Michael J. Kaufman

*Department of Physics, San Jose State University  
One Washington Square, San Jose, CA 95192-0106;  
kaufman@ism.arc.nasa.gov*

## ABSTRACT

The gas at the surfaces of molecular clouds in galaxies is heated and dissociated by photons from young stars both near and far. H I resulting from the dissociation of molecular hydrogen H<sub>2</sub> emits hyperfine line emission at 21 cm, and warmed CO emits dipole rotational lines such as the 2.6 mm line of CO(1–0). We use previously developed models for photodissociation regions (PDRs) to compute the intensities of these H I and CO(1–0) lines as a function of the total volume density  $n$  in the cloud and the far ultraviolet flux  $G_0$  incident upon it and present the results in units familiar to observers. The intensities of these two lines behave differently with changing physical conditions in the PDR, and, taken together, the two lines can provide a ground-based radio astronomy diagnostic for determining  $n$  and  $G_0$  separately in distant molecular clouds. This diagnostic is particularly useful in the range  $G_0 \lesssim 100$ ,  $10 \text{ cm}^{-3} \lesssim n \lesssim 10^5 \text{ cm}^{-3}$ , which applies to a large fraction of the volume of the interstellar medium in galaxies. If the molecular cloud is located near discrete sources of far-UV (FUV) emission, the PDR-generated H I and CO(1–0) emission on the cloud surface can be more easily identified, appearing as layered “blankets” or “blisters” on the side of the cloud nearest to the FUV source. As an illustration, we consider the Galactic object G216 -2.5, i.e. “Maddalena’s Cloud”, which has been previously identified as a large PDR in the Galaxy. We determine that this cloud has  $n \approx 200 \text{ cm}^{-3}$  and  $G_0 \approx 0.8$ , consistent with other data.

*Subject headings:* atomic processes – galaxies: ISM – ISM: atoms – ISM: clouds – ISM: molecules – molecular processes

## 1. Introduction

The interstellar medium (ISM) in galaxies is excited, dissociated, and ionized by far-ultraviolet (FUV) photons produced by young O and B stars. Atomic gas in the ISM recombines into molecular form mainly through the catalytic action of dust grain surfaces. In particular, hydrogen nuclei in the ISM cycle repeatedly from the molecular ( $\text{H}_2$ ) to the atomic (HI) phase and back again, at rates depending on the incident FUV flux  $G_0$ , the total volume density  $n$  of the gas, and the dust-to-gas ratio  $\delta$ . Regions in the ISM where the physics is dominated by FUV photons are called photodissociation regions (PDRs). The surfaces of giant molecular clouds (GMCs) are important (and ubiquitous) examples of PDRs in galaxies.

The physics of PDRs has been explored in detail over the past  $\sim 30$  years by many workers including D. J. Hollenbach, B. T. Draine, A. Dalgarno, J. H. Black, A. G. G. M. Tielens, E. van Dishoeck, J. Le Bourlot, and their students and collaborators. One major focus of this work has been to explain the  $\approx 1\%$  line-to-continuum ratios of the far-infrared lines of [CII] and [OI] in Galactic sources observed from high-altitude aircraft and balloon platforms. With the advent of more sensitive space-based observations, the models were extended to include the weak rotational-vibrational spectrum of excited  $\text{H}_2$  observed on the active PDR surfaces of GMCs that are exposed to relatively intense FUV fluxes from nearby young stars. An excellent review of the observational and theoretical state of the field is given by Hollenbach & Tielens (1999).

PDR model computations have become very detailed and comprehensive, raising the possibility that observations of multiple spectral lines including those from trace molecules such as CO can be used to "invert" the models in order to determine physical conditions in the ISM. For example, a set of such models has been computed by Kaufman et al. (1999) for use in the interpretation of far-infrared and submillimeter spectra from Galactic and extragalactic sources. However, we wish to point out that, although there is qualitative agreement on most of the physics, there are differences in the details of the various model codes currently in use around the world as well as differences in the numerical values of the parameters adopted.

These differences can lead to disagreements in the values derived for physical conditions even for the same observational data: an example of such differences is illustrated in Li et al. (2002). Efforts are underway to intercompare models from different groups in a more systematic manner (E. van Dishoeck 2003, private communication). The results obtained from any one model computation (such as the one we use here) can therefore be revealing in general, but the specific numerical values obtained should be taken with some caution.

The purpose of the present paper is to draw attention to the fact that the HI produced from photodissociated  $\text{H}_2$  can also be a useful diagnostic for determining physical conditions in PDRs. In particular, the combination of the 21 cm HI and 2.6 mm CO(1–0) lines provides a means of independently estimating  $n$  and  $G_0$  in distant PDRs using ground-based radio astronomy data. These two radio lines form a diagnostic that is particularly useful in the area of parameter space where  $G_0 \lesssim 100$ ,  $10 \text{ cm}^{-3} \lesssim n \lesssim 10^5 \text{ cm}^{-3}$ ; this range of FUV flux and total density is representative of most of the volume of the ISM in galaxies.

## 2. PDR Models

Our point of departure is the paper by Kaufman et al. (1999) that describes the results of steady state computations on a specific, extensive set of PDR models over a wide range of physical conditions. These models are simple one-dimensional semi-infinite slabs of gas with constant density  $n = n(\text{HI}) + 2n(\text{H}_2)$  of H nuclei subjected to an equivalent one dimensional flux of FUV photons  $G_0$  measured in units of  $1.6 \times 10^{-3} \text{ ergs cm}^{-2} \text{ s}^{-1}$  over the photon energy range 6–13.6 eV.<sup>1</sup> The line brightness is calculated along a ray normal to the surface of the slab. See Kaufman et al. (1999) for further details of their models.

### 2.1. 2.6 mm CO(1–0) Line Emission

The incident FUV flux dissociates and heats the cloud surface. At some depth into the cloud, the dissociation rate has decreased enough to allow CO molecules to survive, and the density and

---

<sup>1</sup>In these units, the average interstellar radiation field over  $4\pi \text{ sr}$  is  $G_0 \approx 1.7$  (Draine (1978), see our Appendix B and Draine's Fig. 3).

heating rate are still high enough to excite rotational line emission from these molecules. Among many important results, Kaufman et al. (1999) have computed the 2.6 mm CO(1–0) brightness,  $I_{\text{CO}}$ , emanating from the cloud surface; this is the most widely studied molecular line in the ISM. In Figure 1a we present their results for  $I_{\text{CO}}$  as a contour diagram of constant surface brightness (see their Fig. 11); we have extended the range of  $n$  and  $G_0$  down to 1 and 0.03, respectively, and labeled the contours with their original “theoretical” units of  $\text{ergs cm}^{-2} \text{s}^{-1} \text{sr}^{-1}$ , as well as with “CO observer” units of  $\text{K km s}^{-1}$ . This latter conversion is made according to:

$$T_{\text{mb}} \times \Delta V = \frac{\lambda^3}{2k_{\text{B}}} I_{\text{CO}} = 6.4 \times 10^8 \times I_{\text{CO}}, \quad (1)$$

where  $T_{\text{mb}}$  is the measured emergent Rayleigh-Jeans brightness temperature assuming the cloud is completely resolved,  $\Delta V$  is the profile velocity width in  $\text{km s}^{-1}$ ,  $\lambda = 2.60 \text{ mm}$ , and  $k_{\text{B}}$  is Boltzmann’s constant.

We note that Figure 1 assumes that the dust-to-gas ratio  $\delta$  is that of the local ISM near the Sun, and only one side of the slab contributes to the observed emission. A further caution concerns the value of the density  $n$  inferred from a specific observed value of the CO(1–0) intensity in Figure 1a. There is a general trend in most PDR models to underestimate the CO abundance, so that the density inferred from a given observed value of the CO(1–0) line is often higher than that obtained from other independent diagnostics. This is another example in which comparisons among the different modeling efforts will be very useful.

The CO(1–0) surface brightness in Figure 1a is governed by a complex interplay of processes involving the dissociation and reformation of CO molecules, heating and cooling in the ISM, and the detailed excitation and macroscopic radiative transfer of the CO(1–0) line. By contrast, the 21 cm H I line intensity is somewhat easier to compute, since in general this line is optically thin and independent of the kinetic temperature of the ISM; we can therefore ignore the physics of the 21 cm line formation and simply compute the amount of H I produced.

## 2.2. 21 cm H I Line Emission

Incident FUV photons in the wavelength range 912–1108 Å (13.6–11.2 eV) also dissociate the H<sub>2</sub> on the surface of the GMC.<sup>2</sup> This process was first described in the literature by Stecher & Williams (1967) and is by now well known: it has been summarized by Hollenbach & Tielens (1999), who also provide several other references. The dissociated H<sub>2</sub> creates a “blanket” of atomic gas on the surface of the GMC; the H I atoms recombine into H<sub>2</sub> on dust grains and are then returned to the gaseous ISM. Approximate analytic expressions for the steady state column density  $N(\text{H I})$  of the atomic gas have been derived by several authors under a variety of limiting assumptions (e.g. Sternberg (1988); Goldschmidt & Sternberg (1995)) and are discussed in more detail in Appendix A. Computations of  $N(\text{H I})$  in the context of the present “standard model” were first presented in Wolfire et al. (1990) (see their Fig. 6). An updated calculation using the latest code and the model parameters in Kaufman et al. (1999) is presented as the dotted curves in Figure 3. The results differ slightly from those of Wolfire et al. (1990), owing to small differences in the assumed values of dust abundance, atomic abundances, and a different H<sub>2</sub> formation rate. This leads to changes in the depth of the H I – H<sub>2</sub> transition, and hence to different values of  $N(\text{H I})$ ; the differences are, however, generally less than about a factor of 2.

A problem arises in attempting to combine the computational results for CO(1–0) with those for H I. The “standard model” used here is bathed in a uniform flux of cosmic rays producing a constant ionization rate<sup>3</sup> of  $1.8 \times 10^{-17} \text{ s}^{-1}$ . These cosmic rays also produce a faint extended distribution of H I atoms owing mainly to ion chemical reactions everywhere in the cloud. However, as we see below, such a faint extended distribution of H I will in general be removed from the observations by the data reduction process, so we would prefer to use models for  $N(\text{H I})$  *without* a cosmic-ray component. Nevertheless, cosmic-ray ionization is important for the chemistry in the model, thereby

<sup>2</sup>Photons with energies as low as 6.6 eV can also contribute to the dissociation at high FUV flux levels of  $G_0 \gtrsim 10^4$  (Shull 1978).

<sup>3</sup>This parameter is unfortunately missing from Table 1 of Kaufman et al. (1999).

controlling to some extent the abundance of CO molecules, so we ought to keep it in the computations of the CO(1–0) line.

As a compromise we have chosen to use the approximate analytic expression for  $N(\text{HI})$  since it does not include any effects of cosmic rays. This approximation is presented in Appendix A where it is compared with the standard computational model: it is an excellent fit to the model over the full range of parameter space important for this paper and provides a better context in which to compare the theory with the observations. The adopted result for the HI column is shown in Figure 1b.

The conversion from HI column density in Figure 1b to 21 cm emission intensity in  $\text{K km s}^{-1}$  is:

$$T_{\text{mb}} \times \Delta V = 5.5 \times 10^{-19} \times N(\text{HI}), \quad (2)$$

for  $N(\text{HI})$  in units of atoms  $\text{cm}^{-2}$ , and assuming the optical depth of the atomic gas to the 21 cm line radiation is small.

A noteworthy feature of Figure 1b is *the constancy of  $N(\text{HI})$  for a constant ratio of  $G_0/n$*  (see also eq. A2); the same HI column density can be produced in high FUV flux, high-density environments or in low FUV flux, low-density environments. In addition, *the HI column decreases with increasing density at a given value of FUV flux*: this occurs because the destruction rate for  $\text{H}_2$  varies as  $n$ , but the formation rate varies as  $n^2$  (since the grain density is proportional to  $n$ ).

### 2.3. A Combined Model

Figures 1a and 1b show that the contours of constant CO(1–0) emission  $I_{\text{CO}}$  and constant HI column density  $N(\text{HI})$  behave in a complementary fashion. This suggests that over much of the  $n$ – $G_0$  plane an observational determination of  $I_{\text{CO}}$  and  $N(\text{HI})$  for the same PDR would permit independent estimates to be made of both  $n$  and  $G_0$ . In Figure 2 we show the two model computations from Figures 1a and b superposed, along with several additional contours and a “box,” which will be discussed further below.

#### 2.3.1. Range of Validity of the Models

The models become progressively less reliable in the top left corner of the plots for both  $I_{\text{CO}}$  and  $N(\text{HI})$ . This occurs because the assumption of

a steady state model becomes increasingly unreliable in the high  $G_0$  – low  $n$  section of the diagram; in this region, radiation pressure causes grains to drift with speeds of the same order as the gas turbulence speeds (see Kaufman et al. (1999), Fig. 2). Furthermore, this is also the area of the diagram where large HI column densities are predicted; however, values of  $N(\text{HI})$  in excess of a few  $\times 10^{21} \text{ cm}^{-2}$  are not likely to be observed since the 21 cm line may become optically thick in this regime:

$$\begin{aligned} N(\text{HI}) &= 1.82 \times 10^{18} \int_{-\infty}^{\infty} T_s \tau(v) dv \\ &\rightarrow 1.82 \times 10^{18} T_s \tau \Delta v \\ &\approx \text{a few} \times 10^{21} \text{ cm}^{-2}, \end{aligned}$$

for spin temperatures of  $T_s \approx 50 - 100 \text{ K}$ , profile FWHMs of  $\Delta v \approx 4 - 8 \text{ km s}^{-1}$ , and  $\tau \approx 2 - 3$ , values that probably represent the extremes typical for the observations.

#### 2.3.2. Resolution Effects

It should be emphasized that the present calculations of surface brightness can be applied directly only to observations for which the sources of emission are resolved. In any realistic situation, the emission probably arises from several PDR surfaces. In this case, the density and FUV intensity derived from our model using observations of  $I_{\text{CO}}$  and  $N(\text{HI})$  represent ensemble averages of the distribution of values for  $n$  and  $G_0$ . Wolfire et al. (1990) have shown that these averages are somewhat biased toward higher FUV fields; bias toward high or low density depends on the cloud distribution.

#### 2.3.3. Interpretation of $n$

The x axis of Figure 2 refers to the total volume density in our computational model of an isopycnic cloud. In a real GMC this is likely to be close to the actual density at the depth in the cloud where the CO(1–0) line is formed. However, it is not likely to be representative of the density of dissociated HI. This is because the various heating processes at the surface of the GMC (including photodissociation) will lead to gradients in temperature and, therefore, if the pressure is roughly constant, to gradients in density. For example, the

model computations of Allen et al. (1995) for relatively low FUV fluxes<sup>4</sup> of  $G_0 \approx 0.1$  show that the density at the CO(1–0)-emitting layer is about 5 times that at the H I – H<sub>2</sub> interface. Their Figure 4 shows that the CO emission emanates from a depth such that  $A_V \gtrsim 2$ , where the temperature is just below 5 K (see their Fig. 3b), whereas their Figure 2 shows the H I – H<sub>2</sub> interface is effectively at very small values of  $A_V \approx 10^{-3}$ , where the temperature is about 25 K. We have calculated temperatures for higher FUV flux levels  $G_0 = 3$ : the surface temperatures are higher in this case,  $\approx 60$  K at the H I – H<sub>2</sub> interface, and  $\approx 7.5$  K at the CO emission layer, for a ratio of  $\approx 8$ . This ratio will continue to rise for yet higher photon fluxes, since the increased surface heating will result in further increases in surface temperature, but the increase in temperature deeper in the clouds where the CO(1–0) emission is formed will be less rapid because of more effective cooling. If the density and temperature are linked by an isobaric condition, the density observed in the bulk of the H I may be a factor of 5–10 lower than that inferred for the CO(1–0) line.

It is clear from this discussion that constant-density models for PDRs such as the one we have assumed here are not likely to be very realistic. More sophisticated models, for example assuming pressure equilibrium, or a full computation with various forms of micro- and macro-turbulent pressure (e.g., Wolfire et al. (1993)) over the range of the  $G_0$ - $n$  parameter space may provide more realistic results and ought to be explored.

### 3. Discussion

#### 3.1. Complementarity

Figure 2 clearly shows the complementarity of 21 cm H I and 2.6 mm CO(1–0) radio line emission as diagnostics of PDRs. Over the range of validity of our calculations, the CO(1–0) line brightness  $I_{\text{CO}}$  depends mostly on the volume density of the gas for  $n \lesssim 10^3 \text{ cm}^{-3}$ , no matter how intense

<sup>4</sup>The symbol  $\chi$  used by Allen et al. to denote the FUV flux has very nearly the same value as we use here,  $\chi = G_0/0.85$  for irradiation over  $2\pi$  sr. See Appendix B for a discussion of the various definitions of FUV values used in the literature on PDRs.

the FUV flux.<sup>5</sup> On the other hand, for constant  $n$  the H I brightness increases nearly linearly with increasing FUV fluxes up to  $G_0 \approx 10$ –100, becoming logarithmic for higher FUV fluxes. Accordingly, the combination of measurements of  $N(\text{H I})$  and  $I_{\text{CO}}$  from the same PDR can provide unique values for  $n$  and  $G_0$  over a substantial range in the diagram.

#### 3.2. Identifying the Relevant H I and CO Emission

How can extraneous emission from gas that lies far outside the cloud be identified? The spatially layered structure of PDRs provides a direct clue, as has been convincingly shown e.g. by the observations of the Orion Bar region (see Fig. 2 in Hollenbach & Tielens (1999)) on the  $\sim 1$  pc scale. A more or less edge-on viewing angle is required for a certain identification, and one ought to remove any extended emission that is associated with other clouds along the line of sight or produced by other excitation mechanisms. Galaxies that are viewed at low to intermediate inclination angles are favorably oriented for this identification to work, and Allen et al. (1997) and Smith et al. (2000) have shown that the signature morphology can be found at 100 pc scales in the highest resolution H I images of nearby galaxies M81 and M101. As to the CO, it is generally assumed that this arises in PDRs, although the morphological signature is not always clear.

#### 3.3. G216 -2.5: An Example

Figure 2 provides a method for determining  $n$  and  $G_0$  for a specific PDR if  $N(\text{H I})$  and  $I_{\text{CO}}$  can be determined observationally. As an example, we consider the Galactic object G216 -2.5 (also called “Maddalena’s Cloud”) which has been proposed to be a large PDR in the Galaxy by Williams & Maddalena (1996).

##### 3.3.1. H I Column Density

Determining the column density of that part of the H I associated with G216 -2.5 is made quite

<sup>5</sup>The insensitivity of  $I_{\text{CO}}$  to the FUV flux comes about because increasing  $G_0$  merely leads to more photodissociation of the surface CO, and the CO-emitting layer retreats deeper into the static cloud where the temperatures are about the same as they were for the case of lower  $G_0$ .

difficult by confusion from unassociated H I superposed along the line of sight through the Galaxy. Several estimates can be made from the single-dish observations reported by Williams & Maddalena (1996). First, and perhaps simplest, we estimate that fraction of the total averaged H I profile shown in their Figure 1 that is in the velocity range of the CO(1-0) emission (also shown on the same figure); the H I profile shows three overlapping peaks and integrates to  $\approx 48 \text{ K} \times 58 \text{ km s}^{-1} \approx 2800 \text{ K km s}^{-1} = 5.1 \times 10^{21} \text{ cm}^{-2}$ . The averaged  $I_{\text{CO}}$  profile corresponds to the central H I peak and is  $8.5 \text{ km s}^{-1}$  wide (Maddalena & Thaddeus 1985), so the average amount of H I column associated with the CO emission is, by this estimate, probably not more than  $\approx (8.5/58) \times 5.1 \times 10^{21} = 7.5 \times 10^{20} \text{ cm}^{-2}$ . In their §3.2.2, Williams & Maddalena (1996) carry out a more involved analysis with area integrations of the H I in the velocity range  $16\text{--}38 \text{ km s}^{-1}$  and conclude that the “excess” H I associated with the PDR is  $\approx 2 \times 10^{20} \text{ cm}^{-2}$ ; the uncertainty in this method is approximately a factor of 2 (R. Maddalena 2002, private communication). A value in the range  $1 - 8 \times 10^{20} \text{ cm}^{-2}$  may therefore be considered typical for this cloud, with some preference for the lower end of that range.

### 3.3.2. CO(1-0) Intensity

From Figure 1 of Williams & Maddalena (1996), the total  $I_{\text{CO}}$  profile over the whole cloud integrates to  $\approx 7.1 \text{ K km s}^{-1}$ . The CO(1-0) map for the cloud integrated over the same velocity range of  $16\text{--}38 \text{ km s}^{-1}$  as the H I is shown in Figures 2 and 4 of Williams & Maddalena (1996), based on earlier data of Maddalena & Thaddeus (1985).<sup>6</sup> From Figure 2 of Williams & Maddalena (1996) the CO(1-0) brightness ranges from 3–7 contours with a few positions reaching 10 contours. A range of 3–8 contours or  $6\text{--}16 \text{ K km s}^{-1}$  therefore seems representative of the CO data, again with some preference for the lower end of that range.

<sup>6</sup>Note that the  $l-b$  maps in Williams & Maddalena (1996) are similar in shape but brighter by about a factor of 2 when compared to the earlier map of  $I_{\text{CO}}$  in Fig. 2 of Maddalena & Thaddeus (1985). This is not likely to be an effect of differences in the velocity range over which the data have been integrated, since that range is smaller than the range of  $15\text{--}40 \text{ km s}^{-1}$  used by Maddalena & Thaddeus. We use the more recent results of Williams & Maddalena.

### 3.3.3. $n$ and $G_0$ for G216 -2.5

The range of values for  $I_{\text{CO}}$  and  $N(\text{H I})$  obtained above is plotted as a black box on our Figure 2. In the context of our model, these values describe gas with a density range of  $0.7 - 5 \times 10^2 \text{ cm}^{-3}$  and an incident FUV flux of  $0.1\text{--}7$  of the standard value  $G_0$  near the Sun, with likely values being approximately  $2 \times 10^2 \text{ cm}^{-3}$  and  $0.8$ , respectively.

Although no independent measurements of the total volume density are available for G216 -2.5, the value we have obtained is in the range generally indicated for GMCs in the Galaxy ( $n = n(\text{H I}) + 2n(\text{H}_2) \approx 2n(\text{H}_2) \sim 2 \times 50 \text{ cm}^{-3}$ , e.g., Blitz (1993)). As to the FUV flux, Williams & Maddalena (1996) estimated  $G_0 \approx 1$  from what is known about the two nearby young stars identified in their study as likely to be responsible for the photodissociation. Our model thus agrees well with the observations.

### 3.4. Approximate Detection Limits for H I and CO(1-0)

The practical detection limits for the H I 21 cm line are  $\approx 5$  and  $\approx 100 \text{ K km s}^{-1}$  for single-dish survey and interferometer array imaging observations, respectively, corresponding to  $N(\text{H I}) \approx 1 \times 10^{19}$  and  $2 \times 10^{20} \text{ cm}^{-2}$ . These are shown as the dashed (single-dish survey) and dotted (interferometer array) lines for  $N(\text{H I})$  on Figure 2. The corresponding values for the 2.6 mm CO line are  $\approx 1 \text{ K km s}^{-1}$  (dashed line: single dish survey) and  $\approx 10 \text{ K km s}^{-1}$  (dotted line: interferometer array). In all cases, this assumes that the gas clouds are resolved; otherwise these limits need to be increased further by the ratio of the beam area to the cloud area.

Locating the detection limits on our Figure 2, we can conclude that the range in parameter space over which the combination of H I and CO(1-0) can provide useful constraints on  $n$  and  $G_0$  is given approximately by  $G_0 \lesssim 100$ ,  $10 \text{ cm}^{-3} \lesssim n \lesssim 10^5 \text{ cm}^{-3}$ . These boundaries are set by the decreasing sensitivity of the H I emission at high FUV flux levels ( $N(\text{H I})$  increases only logarithmically for high  $G_0$  at constant  $n$ ) and by observational detection limits ( $I_{\text{CO}}$  disappears at low  $n$  owing to insufficient excitation of the transition; H I disappears at high  $n$  as the gas stays mostly molecular).

### 3.4.1. Working with Synthesis Imaging Data

Many observers who report synthesis imaging (interferometer array) data in the literature use units of  $\text{Jy beam}^{-1}$  instead of K. The required conversion factors are (unfortunately) telescope dependent; Appendix C provides an approximate recipe for these conversions.

## 3.5. Conclusions

We have shown that a combination of observations in the 21 cm line of HI and the 2.6 mm line of CO can provide a useful diagnostic for physical conditions in distant PDRs. Both of these lines are readily observed in the Galaxy and in nearby galaxies using ground-based single-dish and interferometer-array radio telescopes. The useful range in parameter space for this combined radio line diagnostic is approximately bounded by  $G_0 \lesssim 100$ ,  $10 \text{ cm}^{-3} \lesssim n \lesssim 10^5 \text{ cm}^{-3}$ , a range that covers a large fraction of the volume of the ISM in galaxies. The unique layered morphology of the emission in PDRs provides a means of identifying that part of the HI and CO emission that is related when that morphology is observable, but confusion along the line of sight makes this separation difficult in the Galaxy. This method will be especially useful for the interpretation of high-resolution HI and CO synthesis imaging data in nearby galaxies where the PDR morphology can be more easily identified.<sup>7</sup> Improvements in the model parameters and in the details of the computations are anticipated in the near future that will permit even more precise values of  $G_0$  and  $n$  to be obtained.

We are grateful to Bruce Draine and David Hollenbach for discussions on the physics of PDRs. David also provided very helpful comments on earlier drafts of this paper. The referee offered many useful suggestions that have also been incorporated.

---

<sup>7</sup>However, in this “extragalactic” case, the effects of beam-smearing are severe and must be carefully considered in relating the observational parameters of the models to the measured brightnesses and profile velocity widths.

## A. COMPARISON OF ANALYTIC AND NUMERICAL MODELS FOR H I PRODUCTION IN PDRs

The H I column density in a PDR is calculated with the same physics used to determine the excitation of the H<sub>2</sub> near-infrared fluorescence lines. A logarithmic form for the analytic solution to the equation for formation–destruction equilibrium was first given by Sternberg (1988) (see also eq. A2 in Hollenbach et al. (1991)<sup>8</sup> and eq. 3 in Goldschmidt & Sternberg (1995)). The model is a simple semi-infinite slab geometry in statistical equilibrium with FUV radiation incident on one side. The solution gives the steady state H I column density along a line of sight perpendicular to the face of the slab as a function of  $\chi$ , the incident UV intensity scaling factor (see Appendix B), and the total volume density  $n$  of H nuclei. Sternberg’s result is:

$$N(\text{H I}) = \frac{1}{\sigma} \times \ln \left[ \frac{DG}{Rn} \chi + 1 \right], \quad (\text{A1})$$

where;

$D$	= the unattenuated H <sub>2</sub> photodissociation rate in the average ISRF,	$R$	= the H <sub>2</sub> formation rate coefficient on grain surfaces,
$\sigma$	= the effective grain absorption cross section per H nucleus in the FUV continuum,	$\chi$	= the incident UV intensity scaling factor,
$N(\text{H I})$	= the H I column density,	$n$	= the volume density of H nuclei.

Equation A1 has been developed using a simplified three-level model for the excitation of the H<sub>2</sub> molecule and is applicable for low-density ( $n \lesssim 10^4 \text{ cm}^{-3}$ ), cold ( $T \lesssim 500 \text{ K}$ ), isothermal, and static conditions, and neglects contributions to  $N(\text{H I})$  from ion chemistry and direct dissociation by cosmic rays. The quantity  $G$  here (not to be confused with  $G_0$  used previously) is a dimensionless function of the effective grain absorption cross section  $\sigma$ , the absorption self-shielding function  $f$ , and the column density of molecular hydrogen  $N_2$ :

$$G = \int_0^{N_2} \sigma f e^{-2\sigma N_2'} dN_2'.$$

The function  $G$  becomes constant for large values of  $N_2$  due to self-shielding (Sternberg 1988). Using the parameter values in this equation adopted by Madden et al. (1993), we have:

$$N(\text{H I}) = 5 \times 10^{20} \times \ln[1 + (90\chi/n)]$$

where  $n$  is in  $\text{cm}^{-3}$ . This is a steady state model, with H<sub>2</sub> continually forming from H I on dust grain surfaces, and H I continually forming from H<sub>2</sub> by photodissociation. In order to compare this result with the “standard model” computations we need to relate  $\chi$  to the  $G_0$  used by Kaufman et al. (1999); this is because Sternberg (1988) and Kaufman et al. (1999) use different normalisations for the FUV flux (see Appendix B). When distributed sources illuminate an FUV-opaque PDR over  $2\pi$  sr, the conversion is  $\chi = G_0/0.85$  (see Footnote 7 in Hollenbach & Tielens (1999)), resulting in  $90\chi/n = 106G_0/n$ .

We have fitted the analytic expression for  $N(\text{H I})$  to the model computations in the range in which cosmic ray dissociation is not a major contributor, roughly for  $G_0 \gtrsim 1$ ,  $n \gtrsim 10 \text{ cm}^{-3}$ . The result is that no consistent improvement is obtained by using any value for the coefficient of  $G_0$  other than the value 106 deduced above, although a modest improvement is obtained by using a slightly larger value for the leading coefficient in the equation,  $7.8 \times 10^{20}$ , corresponding to a value of  $1.3 \times 10^{-21} \text{ cm}^2$  for the effective grain absorption cross section. With these small adjustments, our final equation is:

$$N(\text{H I}) = 7.8 \times 10^{20} \times \ln[1 + (106G_0/n)] \text{ cm}^{-2}, \quad (\text{A2})$$

<sup>8</sup>David Hollenbach has kindly pointed out to us that there is a typographical error in eq. A1 of their paper; the right side should read  $I_0(\beta/N_2^{0.5})n_2e^{-KN}$ .

resulting in an  $r^2$  value for the fit that is everywhere in excess of 99% over the fitted range of  $n$  and  $G_0$ .

In Figure 3 we show values from equation A2 plotted as solid lines together with dotted contour lines from our standard numerical model. The agreement is generally good over much of the  $n$ - $G_0$  parameter space of interest here; differences occur mainly in the top left corner of the diagram, and at low values of FUV flux. In the top left corner the analytic formula under-predicts the amount of HI column density computed from the standard model by about 30% owing to HI production by ion chemistry reactions such as  $H_2^+ + H_2 \rightarrow H_3^+ + H$ ,  $HCO^+ + e^- \rightarrow CO + H$ , and  $PAH^- + H^+ \rightarrow PAH + H$  (where PAH is a polycyclic aromatic hydrocarbon), which are important at high  $G_0$  and low  $n$ . At values of  $G_0 \lesssim 1$  the contours of  $N(\text{HI})$  for the numerical model become vertical; this is because the standard model includes a low level of cosmic ray ionization (see main text) which contributes a small amount of HI even for  $G_0 = 0$ .

## B. DEFINITIONS OF THE MEAN INTERSTELLAR RADIATION FIELD

Kaufman et al. (1999) characterized the emission from photodissociation regions (PDRs) in terms of the “strength” of the FUV radiation field,  $G_0$ , illuminating the medium at energies between 6 and 13.6 eV. Numerical values for  $G_0$  were presented in units of the “Habing Field,” following earlier PDR modeling by Tielens & Hollenbach (1985), who expressed  $G_0$  in units of the “equivalent Habing (1968) flux of  $1.6 \times 10^{-3}$  ergs  $\text{cm}^{-2}$   $\text{s}^{-1}$  appropriate to the average interstellar medium.” However, other characterizations of the FUV background also appear in the literature for the “typical” and local ISM. Draine (1978) has developed an analytic fit to many of these, which he defined as the “standard UV background” from 5–13.6 eV.

Although numerical values for the Habing (1968) and Draine (1978) representations of the average interstellar background can be interconverted, Draine’s Figure 3 makes it evident that they have different spectral shapes. Furthermore, the “strength” of the interstellar FUV field is described in the literature by several different quantities (e.g., energy density, photon intensity, energy flux) using a variety of units. Some authors use a single symbol to report normalized values of their field descriptor, while others specifically represent the normalized quantity by a ratio. Accordingly, the purpose of this appendix is to summarize the approach taken by Habing and Draine in developing their descriptions of the ISRF at ultraviolet wavelengths and to interrelate the representations of that field adopted by several authors whose work is germane to our paper.

Habing (1968) calculated radiation energy density values,  $u_\lambda$ , at 1000, 1400, and 2200 Å which were averaged “over a considerable area” in space, using bandwidths of 912–1040, 1300–1450, and 1900–2400 Å, respectively. His recommended values for the averaged energy density  $\langle u_\lambda \rangle$  were

$$\begin{aligned} \langle u_\lambda \rangle &= 40 \times 10^{-18} \text{ ergs cm}^{-3} \text{ \AA}^{-1} \text{ at } 1000 \text{ \AA} \text{ (11.9 – 13.6 eV)} \\ &= 50 \times 10^{-18} \text{ ergs cm}^{-3} \text{ \AA}^{-1} \text{ at } 1400 \text{ \AA} \text{ (8.6 – 9.5 eV)} \\ &= 30 \times 10^{-18} \text{ ergs cm}^{-3} \text{ \AA}^{-1} \text{ at } 2200 \text{ \AA} \text{ (5.2 – 6.5 eV)} \end{aligned} \tag{B1}$$

However, Habing’s results depend strongly on assumptions made concerning the wavelength dependence of interstellar extinction and the presence of diffuse galactic light. Witt & Johnson (1973) noted that these are “two areas for which there existed little or no observational data at the time of his work.”

Draine (1978) converted these and other existing calculations of the interstellar UV energy density into a quantity that he defined as the angle-averaged photon flux

$$F(E) \equiv \lambda^3 u_\lambda / (4\pi h^2 c) \text{ photons cm}^{-2} \text{ s}^{-1} \text{ sr}^{-1} \text{ eV}^{-1} \tag{B2}$$

where  $E$  is the energy,  $h$  represents Planck’s constant, and  $c$  is the speed of light. The resulting values and a few observational data points are plotted on his Figure 3, together with an analytical expression that is “in good agreement with all of the above results over the range 5–13.6 eV.” That expression,

$$F_D(E) = 1.658 \times 10^6 E - 2.152 \times 10^5 E^2 + 6.919 \times 10^3 E^3 \text{ photons cm}^{-2} \text{ s}^{-1} \text{ sr}^{-1} \text{ eV}^{-1} \tag{B3}$$

where  $E$  is measured in eV, was referred to by Draine as the “standard UV background” in the ISM. Since it is computed on a “per steradian” basis, this quantity is actually an angle-averaged photon intensity.

We have used equation B2 to convert the Habing (1968) energy density values to angle-averaged photon intensities (denoted  $F_H(E)$ ) at the three wavelengths reported in his paper, and they agree well with the corresponding points on Figure 3 of Draine (1978). We have also computed values for Draine’s “standard” UV background at the same wavelengths, using equation B3. At 1000 Å,  $F_H(E) = 3.875 \times 10^5$  photons  $\text{cm}^{-2} \text{s}^{-1} \text{sr}^{-1} \text{eV}^{-1}$ ,  $F_D(E) = 6.627 \times 10^5$  (in the same units), and  $F_H(E)/F_D(E) = 0.585$ . Thus, the photon intensity computed from Draine’s fit at this wavelength is 1.710 times that found by converting Habing’s calculated energy density to these units. This result is identical to the value computed by Draine & Bertoldi (1996) at 1000 Å, and (to one decimal point) to the value given in footnote 7 of Hollenbach & Tielens (1999). The same result could also be obtained by first converting Draine’s photon intensity to an energy density for direct comparison to Habing’s (1968) calculation. Draine & Bertoldi (1996) chose Habing’s result at 1000 Å as the basis for normalization because in “neutral regions, pumping of  $\text{H}_2$  is primarily effected by far-ultraviolet photons in the 1110–912 Å range”. The energy flux over  $4\pi$  sr at 1000 Å is  $F = 4\pi E F_H(E) = 1.2 \times 10^{-3}$  ergs  $\text{cm}^{-2} \text{s}^{-1} = 4\pi \bar{I}$ , where  $\bar{I}$  is the mean intensity.

The values for these quantities at 1400 Å are  $F_H(E) = 1.329 \times 10^6$ ,  $F_D(E) = 2.611 \times 10^6$ , and  $F_H(E)/F_D(E) = 0.509$ . In this case, Draine’s fit to the angle-averaged photon intensity is 1.965 times the converted Habing result, and the energy flux is  $F = 4\pi E F_H(E) = 2.1 \times 10^{-3}$ . At 2200 Å,  $F_H(E) = 3.094 \times 10^6$ ,  $F_D(E) = 3.748 \times 10^6$ , and  $F_H(E)/F_D(E) = 0.826$ . The “standard” Draine result is 1.211 times that calculated by Habing at this wavelength, and the energy flux  $F = 4\pi E F_H(E) = 2.0 \times 10^{-3}$ .

Draine’s standard curve can be integrated from 6 to 13.6 eV to find the total photon intensity, i.e.,  $1.547 \times 10^7$  photons  $\text{cm}^{-2} \text{s}^{-1} \text{sr}^{-1}$ . When this result is multiplied by the average energy per photon (i.e.,  $1.407 \times 10^{-11}$  ergs) over that interval, the Draine flux over  $4\pi$  sr is  $F_D = 2.7 \times 10^{-3}$  ergs  $\text{cm}^{-2} \text{s}^{-1}$ . If we assume that the photon intensity ratio found earlier in the 11.9–13.6 eV band, e.g.,  $F_H(E)/F_D(E) = 0.585$ , applies over the entire FUV spectrum (i.e., 6–13.6 eV), then  $F_H = 1.6 \times 10^{-3}$  ergs  $\text{cm}^{-2} \text{s}^{-1}$ . This is the equivalent Habing flux.

Since both ultraviolet normalization procedures are still used in the literature, confusion can arise when comparing descriptors of the ISRF. Kaufman et al. (1999) represent that field by an “incident FUV flux”,  $G_0$ , that is already normalized by the equivalent Habing flux of the average ISM (see their Table 1). Normalization to the Habing field was also used by Hollenbach & Tielens (1999) and Wolfire et al. (1990). The use of this normalization in these models is purely historical, having been incorporated into early versions of the underlying code in support of PDR modeling begun in the 1980’s (M. Wolfire 1999, private communication).

In contrast, Sternberg (1988) and Sternberg & Dalgarno (1989, 1995) compute the “UV photon intensity” (i.e.,  $\chi I_\nu$ ) by introducing a “UV intensity scaling factor”  $\chi$  which is defined to be unity for Draine’s fit to the average interstellar field intensity  $I_\nu$ . In Sternberg (1988) and Sternberg & Dalgarno (1989), the Draine (1978) standard result is re-expressed as

$$I_\nu = \frac{1.068 \times 10^{-4}}{\lambda} - \frac{1.719 \times 10^{-2}}{\lambda^2} + \frac{6.853 \times 10^{-1}}{\lambda^3} \text{ photons cm}^{-2} \text{ s}^{-1} \text{ Hz}^{-1}, \quad (\text{B4})$$

where  $\lambda$  is expressed in nanometers. When Sternberg’s representation of Draine’s standard background (i.e., eq. B4) is integrated from 6 to 13.6 eV, and the resulting value,  $1.942 \times 10^8$  photons  $\text{cm}^{-2} \text{s}^{-1}$ , is multiplied by the average energy per photon, the total FUV flux over  $4\pi$  sr is  $F_S = 2.7 \times 10^{-3}$  ergs  $\text{cm}^{-2} \text{s}^{-1}$ . Once again, we find that  $F_H = 1.6 \times 10^{-3}$  provided the ratio  $F_H(E)/F_D(E) = 0.585$  found earlier between 11.9 and 13.6 eV (i.e., 912–1040 Å) is assumed to apply over the entire FUV band.

Equation B4 can be obtained from equation B3 by multiplying the latter by  $4\pi$  sr and  $4.136 \times 10^{-15}$  eV  $\text{Hz}^{-1}$ , provided  $E$  is replaced by  $hc/\lambda = 1.240 \times 10^{-3}/\lambda_{nm}$  eV. Thus,

$$I_\nu = 1.654\pi \times 10^{-14} F_D(hc/\lambda_{nm}). \quad (\text{B5})$$

We note that equation B4 represents a photon flux rather than the photon intensity, since it has been averaged over solid angle. Sternberg & Dalgarno (1995) corrected this problem in their equation A1 by multiplying equation B4 by  $1/4\pi$ , resulting in corrected units of photons  $\text{cm}^{-2} \text{s}^{-1} \text{Hz}^{-1} \text{sr}^{-1}$ . When this correction is made, equation B5 becomes  $I_\nu = 4.136 \times 10^{-15} F_D(hc/\lambda_{nm})$ .

Madden et al. (1993) explicitly introduced field normalization through the ratio  $\chi_{UV}/\chi_0$ , where  $\chi_{UV}$  is defined as the UV field intensity, although they also called it an FUV energy flux. Unfortunately, the subscript “UV” is dropped later in their paper where the ratio is shown as  $\chi/\chi_0$ , increasing the potential for equating the numerator (incorrectly) with Sternberg’s parameter  $\chi$  upon casual inspection. The divisor,  $\chi_0 = 2.0 \times 10^{-4} \text{ergs cm}^{-2} \text{s}^{-1} \text{sr}^{-1}$ , was determined from the “UV field” results in the solar neighborhood presented by Draine (1978). Although not explicitly stated when  $\chi_0$  was defined, their introduction identifies the band of interest as extending from 912 - 2000 Å (i.e., 6.2 - 13.6 eV). Over  $4\pi \text{sr}$ , the flux corresponding to the Madden et al. value of  $\chi_0$  is  $F_M = 2.5 \times 10^{-3} \text{ergs cm}^{-2} \text{s}^{-1}$ , and  $F_H = 1.5 \times 10^{-3}$  if we continue to assume that  $F_H(E)/F_D(E) = 0.585$ .

The key issue for this paper is how to relate the dimensionless field descriptor chosen by Kaufman et al. (1999), i.e.,  $G_0$ , to the dimensionless quantity used by Sternberg (1988),  $\chi$ , or by Madden et al. (1993),  $\chi_{UV}/\chi_0$ . Since  $\chi$  was normalized by Draine’s standard background between 6 and 13.6 eV, and  $\chi_0$  was computed by integrating the same curve over a similar energy range (the lower limits may differ by 0.2 eV),  $\chi_{UV}/\chi_0$  is equivalent to  $\chi$ . We illustrate this circumstance by comparing the flux computed earlier from Sternberg’s representation of Draine’s standard curve (i.e., from eq. B4), given by  $F_S = 2.7 \times 10^{-3} \text{ergs cm}^{-2} \text{s}^{-1}$ , with the flux computed (using fewer significant figures) from the value of  $\chi_0$  used by Madden et al. (1993). The latter is  $F_M = 2.5 \times 10^{-3} \text{ergs cm}^{-2} \text{s}^{-1}$ . This conclusion is not affected by whether or not the Sternberg (1988) expression is multiplied by a solid angle factor (i.e.,  $1/4\pi$ ) provided his numerator is multiplied by the same factor.

The dimensionless parameter  $G_0 = [4\pi \int F(E)dE]/[4\pi \int F_H(E)dE]$  is a flux ratio that is computed over the same spectral band as  $\chi_0$ , where the denominator  $\int F_H(E)dE = 0.585 \int F_D(E)dE$  in the highest energy band (i.e., 11.9–13.6 eV) addressed by Habing (1968). Accordingly, over that band  $G_0 = 1.710 \int F(E)dE / \int F_D(E)dE$ . Since  $\chi_0$  (with units of  $\text{ergs cm}^{-2} \text{s}^{-1} \text{sr}^{-1}$ ) represents an intensity that is referenced to Draine’s standard curve, it can be written as  $\int F_D(E)dE$ , whereby  $G_0 = 1.710 \chi_{UV}/\chi_0 = 1.710 \chi$ . Inserting this into equation 12 of Madden et al. (1993), the argument of the logarithm, i.e.,  $[90(\chi_{UV}/\chi_0)/n] + 1$  can be written as  $[53G_0/n] + 1$ , in agreement with equation A2 when the latter is written to accommodate irradiation over  $4\pi \text{sr}$ .

### C. RADIO BRIGHTNESS UNIT CONVERSIONS

It is common practice to report results from imaging synthesis observations of radio spectral lines as contour diagrams of constant surface brightness using “J  $\text{beam}^{-1} \text{km s}^{-1}$ ” as the unit.<sup>9</sup> This unfortunate combination of units is telescope dependent through the use of the beam unit in the denominator. The conversion to telescope-independent units such as K  $\text{km s}^{-1}$  (which we use here in eqs. 1 and 2) requires knowledge of the beam area of the radio telescope in steradians, which is not well defined for any radio synthesis imaging telescope owing to the absence of information at short interferometer spacings. Fortunately (at least for now), most data processing systems perform an image restoration step that sets the final point spread function to be a two-dimensional Gaussian. This provides a definite (but not necessarily accurate) value for the two-dimensional integral over the beam, and thereby “solves” the unit conversion problem. If we take the FWHMs of this Gaussian to be  $\theta_1$  and  $\theta_2$ , then the conversion for 21 cm HI image contours may be done with the relation

<sup>9</sup>Or, quite incorrectly, as “J  $\text{km s}^{-1}$ ” (e.g. Sheth et al. (2002)). Another interesting (and equally erroneous) variant is to give single dish spectra in units of “K  $\text{beam}^{-1}$ ” (e.g. Fig. 4 in Schinnerer & Scoville (2002)).

$$\frac{T_b(\text{HI})}{dS/d\Omega} = \frac{6.057 \times 10^5}{\theta_1 \times \theta_2}, \quad (\text{C1})$$

for  $T_b$  in K,  $dS/d\Omega$  in Jy beam<sup>-1</sup>, and  $\theta_1$  and  $\theta_2$  in arcseconds. The corresponding relation for the 2.6 mm line of CO(1-0) is:

$$\frac{T_b(\text{CO})}{dS/d\Omega} = \frac{91.97}{\theta_1 \times \theta_2}, \quad (\text{C2})$$

with the same units as the previous equation. We emphasize again that these temperatures are well defined only for completely resolved sources. If the telescope beam does not resolve the source, the data can provide only a lower limit to the true brightness; such lower limits are usually called “main beam brightness temperatures” and labelled  $T_{mb}$ .

## REFERENCES

- Allen, R.J., Le Bourlot, J., Lequeux, J., Pineau Des Forêts, G., & Roueff, E. 1995, ApJ, 444, 157
- Allen, R.J., Knapen, J., Bohlin, R., & Stecher, T. 1997, ApJ, 487, 171
- Blitz, L. 1993, in *Protostars & Planets III*, eds. E.H. Levy & J.I. Lunine (Tucson; Univ. Arizona Press), 125
- Draine, B.T. 1978, ApJS, 36, 595
- Draine, B.T., & Bertoldi, F. 1996, ApJ, 468, 269
- Goldschmidt, O., & Sternberg, A. 1995, ApJ, 439, 256
- Habing, H.J. 1968, Bull. Astr. Inst. Netherlands, 19, 421
- Hollenbach, D.J., Takahashi, T., & Tielens, A.G.G.M. 1991, ApJ, 377, 192
- Hollenbach, D.J., & Tielens, A.G.G.M. 1999, Revs. Mod. Phys., 71, 173
- Kaufman, M.J., Wolfire, M.G., Hollenbach, D.J., & Luhman, M.L. 1999, ApJ, 527, 795
- Li, W., Evans, N.J., Jaffe, D.T., van Dishoeck, E.F., & Thi, W.-F. 2002, ApJ, 568, 242
- Maddalena, R.J., & Thaddeus, P. 1985, ApJ, 294, 231
- Madden, S.C., Geis, N., Genzel, R., Herrmann, F., Jackson, J., Poglitsch, A., Stacey, G.J., & Townes, C.H. 1993, ApJ, 407, 579
- Schinnerer, E., & Scoville, N. 2002, ApJ, 577, L103
- Sheth, K., Vogel, S.N., Regan, M.W., Teuben, P., Harris, A.J., & Thornley, M.D. 2002, AJ, 124, 2581
- Shull, J.M. 1978, ApJ, 219, 877
- Smith, D.A., Allen, R.J., Bohlin, R.C., Nicholson, N., & Stecher, T.P. 2000, ApJ, 538, 608
- Stecher, T.P., & Williams, D.A. 1967, ApJ, 149, L29
- Sternberg, A. 1988, ApJ, 332, 400
- Sternberg, A., & Dalgarno, A. 1989, ApJ, 338, 197
- Sternberg, A., & Dalgarno, A. 1995, ApJS, 99, 565
- Tielens, A.G.G.M., & Hollenbach, D. 1985, ApJ, 291, 722
- Williams, J.P., & Maddalena, R.J. 1996, ApJ, 464, 247
- Witt, A.N., & Johnson, M.W. 1973, ApJ, 181, 363
- Wolfire, M.G., Tielens, A.G.G.M., & Hollenbach, D. 1990, ApJ, 358, 116
- Wolfire, M.G., Hollenbach, D., & Tielens, A.G.G.M. 1993, ApJ, 402, 195

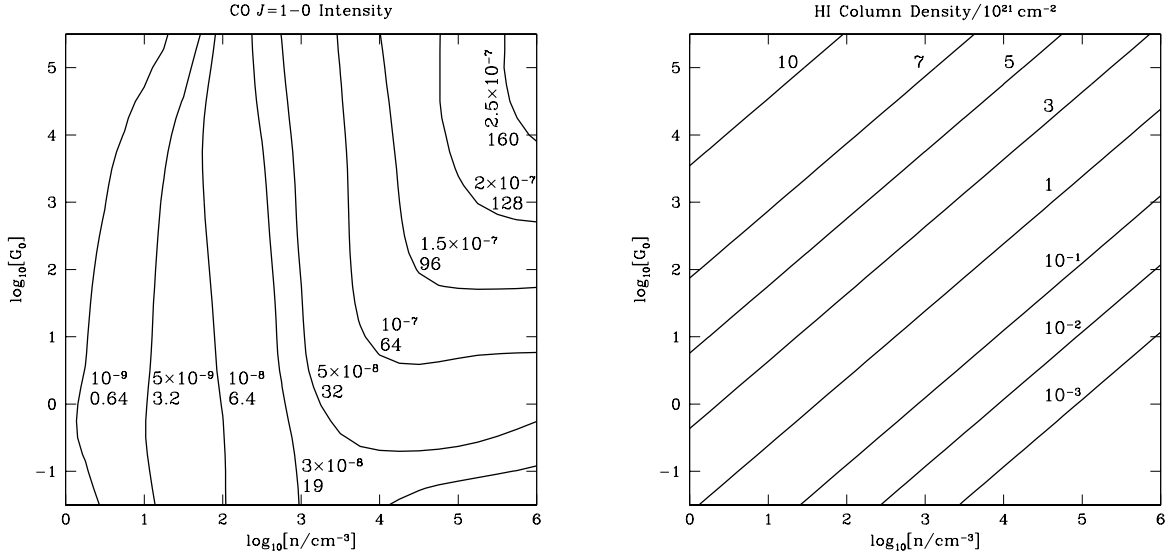


Fig. 1.— a). (left panel) CO(1–0) emission at 2.6 mm from the surface of the model PDR as a function of the density  $n$  and incident FUV flux  $G_0$  for the standard model parameters in Kaufman et al. (1999). The density  $n = n_1 + 2n_2$  is the total density of H in atomic ( $n_1$ ) and molecular ( $n_2$ ) form at the depth where the CO(1–0) line is formed. At this point the gas is essentially all  $\text{H}_2$ . Contours of constant CO(1–0) emission  $I_{\text{CO}}$  are shown, labeled in both ergs  $\text{cm}^{-2}$   $\text{s}^{-1}$   $\text{sr}^{-1}$  and in CO-observer units of  $\text{K km s}^{-1}$ . The PDR is assumed to have the dust-to-gas ratio  $\delta$  of the local ISM near the Sun. b). (right panel) HI column density  $N(\text{HI})$  in units of  $10^{21}$   $\text{cm}^{-2}$  produced by photodissociation in the analytic approximation of eq. A2. This approximation is preferred for comparisons with observational data (see §2.2).

## CO (J=1-0) Intensity and HI Column Density

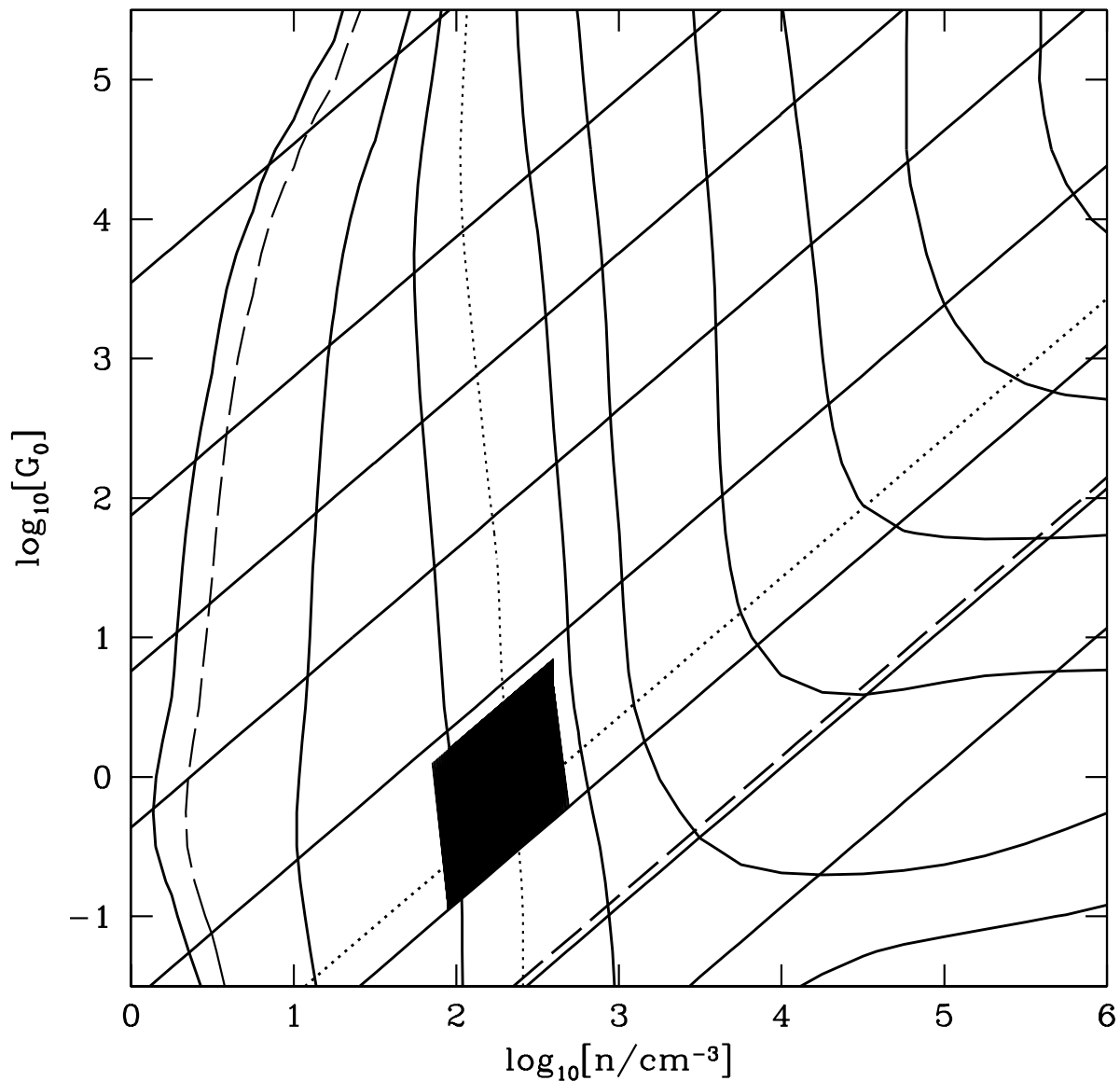


Fig. 2.— Combined plot from the model computations of CO(1-0) emission  $I_{\text{CO}}$  in Fig. 1a and  $N(\text{HI})$  in Fig. 1b. The contour labels, identical with Fig. 1, are omitted here for clarity. Shown are approximate observational limits for single dish (*dashed lines*) and interferometer imaging synthesis data (*dotted lines*). These limits are described in the text §3.4. The black “box” shows the approximate range allowed by the observations of G216 -2.5.

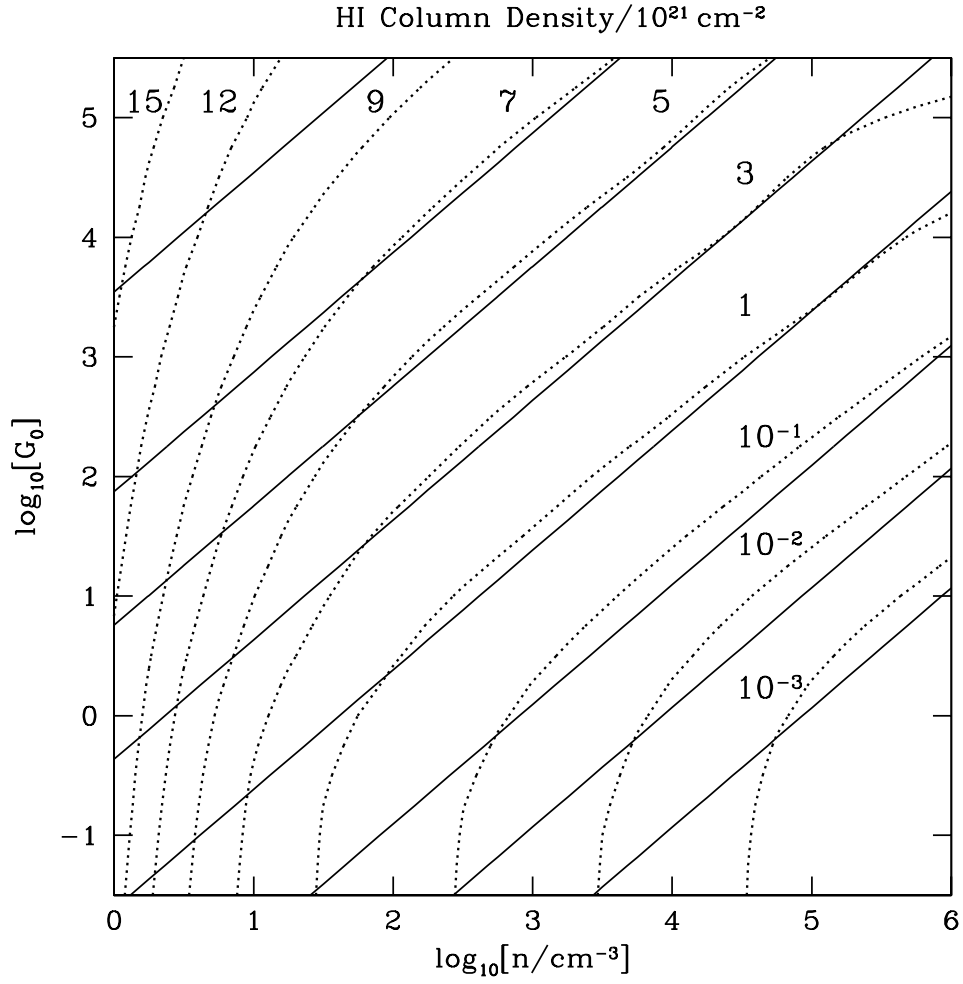


Fig. 3.— Contours of constant HI column density  $N(\text{HI})$  in units of  $10^{21} \text{ cm}^{-2}$  in the PDR as a function of the density  $n$  and incident FUV flux  $G_0$  for the standard model parameters in Kaufman et al. (1999) (*dotted lines*), and for the analytic approximation of eq. A2 (*solid lines*). The labeled contour values are for the numerical model; the contours for the analytic model are as in Fig. 1.